

# Beyond conventional vision: RGB-event fusion for robust object detection in dynamic traffic scenarios

Zhanwen Liu<sup>a,\*</sup>, Yujing Sun<sup>a</sup>, Yang Wang<sup>a</sup>, Nan Yang<sup>a</sup>, Shengbo Eben Li<sup>b</sup>, Xiangmo Zhao<sup>a</sup>

<sup>a</sup> *School of Information Engineering, Chang'an University, Xi'an, 710000, China*

<sup>b</sup> *School of Vehicle Mobility & College of AI, Tsinghua University, Beijing, 100084, China*

\* Corresponding author.

E-mail address: zwliu@chd.edu.cn

## Abstract

The dynamic range limitation is intrinsic to conventional RGB cameras, which reduces global contrast and causes the loss of high-frequency details such as textures and edges in complex, dynamic traffic environments (e.g., nighttime driving or tunnel scenes). This deficiency hinders the extraction of discriminative features and degrades the performance of frame-based traffic object detection. To address this problem, we introduce a bio-inspired event camera integrated with an RGB camera to complement high dynamic range information, and propose a motion cue fusion network (MCFNet), an innovative fusion network that optimally achieves spatiotemporal alignment and develops an adaptive strategy for cross-modal feature fusion, to overcome performance degradation under challenging lighting conditions. Specifically, we design an event correction module (ECM) that temporally aligns asynchronous event streams with their corresponding image frames through optical-flow-based warping. The ECM is jointly optimized with the downstream object detection network to learn task-aware event representations. Subsequently, the event dynamic upsampling module (EDUM) enhances the spatial resolution of event frames to align its distribution with the structures of image pixels, achieving precise spatiotemporal alignment. Finally, the cross-modal mamba fusion module (CMM) employs adaptive feature fusion through a novel cross-modal interlaced scanning mechanism, effectively integrating complementary information for robust detection performance. Experiments conducted on the DSEC-Det and PKU-DAVIS-SOD datasets demonstrate that MCFNet significantly outperforms existing methods in various poor lighting and fast moving traffic scenarios. Notably, on the DSEC-Det dataset, MCFNet achieves a remarkable improvement, surpassing the

best existing methods by 7.4% in mAP50 and 1.7% in mAP metrics, respectively. The code is available at <https://github.com/Charm11492/MCFNet>.

## Keywords

dynamic traffic environments, object detection, multimodal fusion, event camera

## 1 Introduction

Visual perception systems serve as the foundational component enabling intelligent vehicles to perceive surrounding environments and facilitate decision-making (Huang et al., 2024; Liao et al., 2024; Ma and Xue, 2024). These systems must maintain robust performance for object detection in complex, dynamic edge cases such as nighttime driving and tunnel navigation. However, conventional RGB cameras, limited by the narrow dynamic range of their intrinsic photosensitive elements, often struggle to capture critical edge details and rapid scene variations under such challenging conditions. As shown in Fig. 1, this results in degraded image quality, impairing discriminative feature extraction and adversely affecting the accuracy of frame-based traffic object detection methods (Berman and Stern, 2011).

In contrast, bio-inspired event cameras provide a high dynamic range and microsecond-level temporal resolution, allowing for stable imaging under extreme conditions such as low light, and overexposure (Chen and Yu, 2024; Chen et al., 2023; Rizzo, 2024). By harnessing the complementary strengths of RGB and event-based information, multi-modal fusion approaches offer a promising avenue for visual perception in complex traffic environments (Bayoudh et al., 2022). Recently, numerous object detection algorithms have been developed to exploit RGB and event fusion, significantly enhancing the robustness of visual perception systems in challenging scenarios (Cao et al., 2024b; Li et al., 2023; Tomy et al., 2022). These methods typically involve designing dedicated multi-modal representation branches to extract features from each modality and implementing advanced fusion modules to deeply integrate cross-modal information, thereby improving detection performance.

However, the heterogeneity between RGB and event cameras causes spatiotemporal inconsistencies in multimodal data, posing challenges for existing methods in multimodal feature extraction and alignment. First, in the temporal dimension, the microsecond-level temporal resolution of event data is significantly

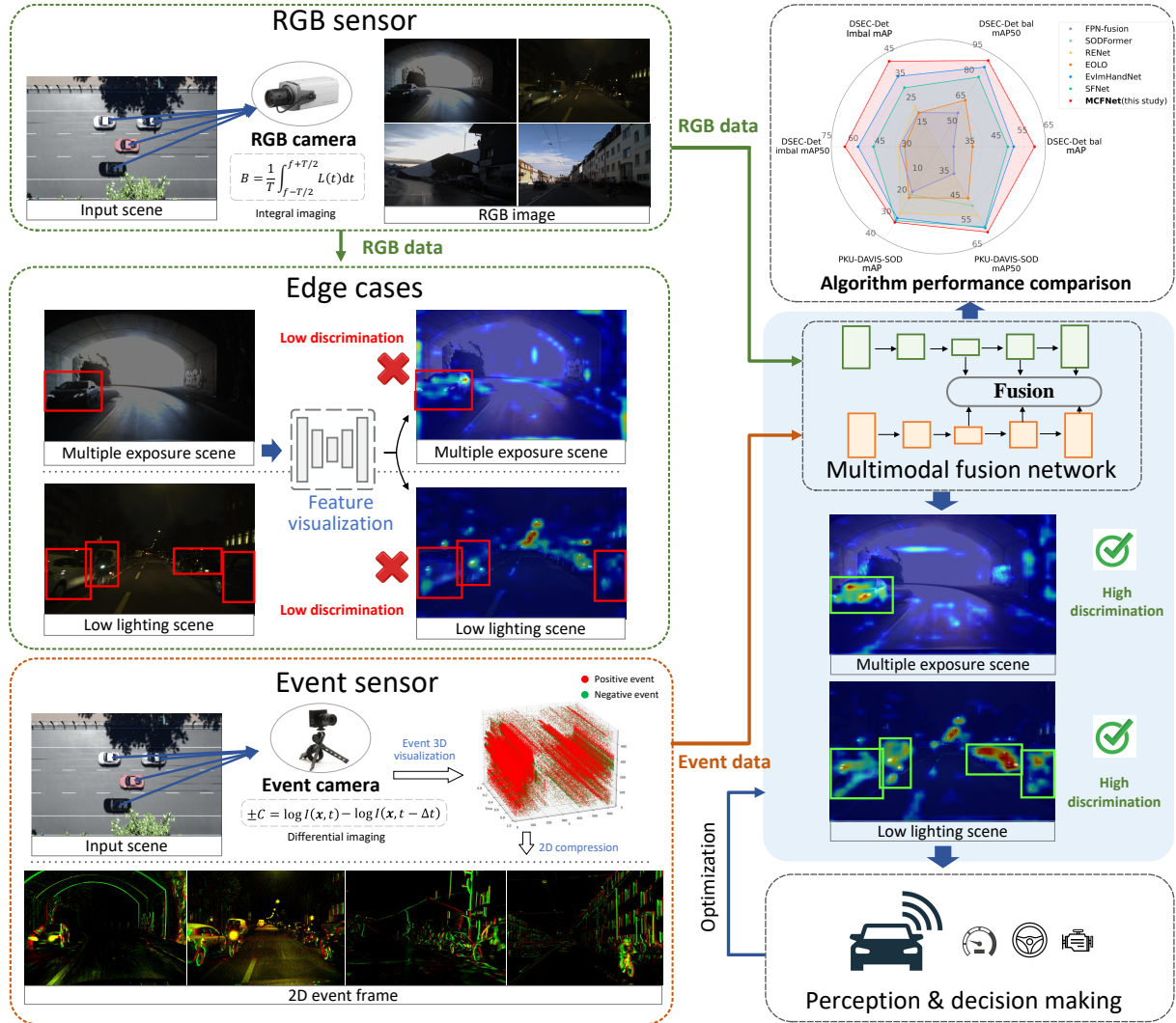


**Fig. 1** Conventional RGB cameras in boundary perception scenarios are limited by their photosensitive elements and fixed frame rates, making them susceptible to the loss of critical information due to insufficient exposure (upper left), which leads to the failure of downstream algorithms. In contrast, event cameras can capture high-dynamic spatiotemporal features even under extreme conditions (lower left). To this end, we propose a multi-modal fusion algorithm that jointly optimizes the complementarity of RGB and event data to construct a cross-modal feature representation and decision-making mechanism (lower right), thereby significantly enhancing the robustness and accuracy of perception for intelligent vehicles in complex scenarios (upper right).

higher than the millisecond-level resolution of RGB data, resulting in temporal misalignment and making direct multimodal fusion infeasible (Gallego et al., 2020). To address this issue, existing methods typically perform temporal sampling and compression on event data to generate event frames that align with the temporal resolution of RGB data. These approaches can be broadly categorized into two types: event frame accumulation methods and motion compensation methods. Event frame accumulation methods generate image-like tensors using statistical features of events (Kim et al., 2021; Maqueda et al., 2018; Park et al., 2016; Zhu et al., 2018a,b), but they are inevitably affected by thermal noise and dark current noise,

which degrade the quality of subsequent structural feature extraction. Motion compensation methods exploit the temporal dynamics of event data to align continuous motion events, thereby enhancing motion regions and forming high-intensity edges while suppressing noise with discontinuous motion. However, these methods (Paredes-Vallés et al., 2021, 2023) rely on assumptions of constant illumination and linear motion, which are often violated in highly dynamic traffic scenarios with frequent brightness variations (e.g., vehicle headlights, streetlights) and complex motion patterns, leading to inaccurate motion estimation and degraded event frame quality (Basha et al., 2013; Brox and Malik, 2010). Second, in the spatial dimension, RGB data typically have much higher resolution than event data, leading to significant significant disparity (Gehrig et al., 2021). Existing methods often address this by directly downsampling RGB data to match the resolution of event data, which further exacerbates information loss (Tomy et al., 2022; Zhou et al., 2023).

After extracting representations from both modalities, the spatial inconsistency of illumination distribution results in different discriminability levels of the two modalities across different regions. This necessitates dynamically balancing the contributions of each modality to achieve robust cross-modal feature fusion. Existing methods typically fuse features of the two modalities through simple addition or concatenation (Cao et al., 2021; Tomy et al., 2022; Yang et al., 2025), which cannot adaptively adjust the fusion ratio based on dynamic scene variations. More recent approaches employ attention mechanisms to capture complementary information (Cao et al., 2024b; Li et al., 2023; Liu et al., 2024b; Zhou et al., 2023). However, they either treat one modality as auxiliary to enhance the other or build separate enhancement submodules for each modality, failing to fully exploit inter-modal collaborative information and hinder precise balancing of modality contributions.

To address the aforementioned challenges, we propose a novel motion cue fusion network (MCFNet), which consists of three main components: the event correction module (ECM) and the event dynamic upsampling module (EDUM) for spatiotemporal alignment between RGB and event data to generate high quality pixel to pixel alignment features, and the cross-modal mamba fusion module (CMM) for global contextual modeling across modalities to guide adaptive fusion. Specifically, ECM estimates the motion vectors of the event stream to temporally align the motion events with the RGB frame timestamps. To overcome the limitations of constant illumination and linear motion, an end-to-end joint training

strategy that leverages high-level semantic information to guide model optimization is employed. This enables the learning of scene features and the generation of event frames with high-intensity edges and robust noise resilience in highly dynamic traffic scenarios. Building upon this, EDUM is introduced to perform dynamic up-sampling by leveraging the spatial distribution of event features and image local smoothness characteristic to suppress noise, yielding high-resolution and high-quality event features. After extracting high-quality spatiotemporally aligned features from both modalities, CMM employs inter-modal global context interactions to perceive scene content and assess each modality's contribution. This guides the adaptive leveraging of either event dynamics or RGB texture features for cross-modal fusion, fully exploiting their complementary characteristics. To validate the effectiveness of MCFNet, we conducted extensive experiments on the DSEC-Det (Gehrig et al., 2021) and PKU-DAVIS-SOD (Li et al., 2023) datasets. As shown in Fig. 1, MCFNet significantly outperforms the existing methods.

In summary, the main contributions of this study are as follows:

- 1) In temporal alignment, an self-supervised learning based event correction module (ECM) is proposed to estimate full-scene optical flow, providing initial values for joint training. Subsequently, ECM is jointly optimized with the detection network to mitigate the influence of constant lighting and linear motion assumption in optical flow, promising high-quality task-aware event representations.
- 2) In spatial alignment, a novel event dynamic upsampling module(EDUM) is devised to extract RGB feature smoothness properties to suppress noise amplification during event representation up-sampling, guaranteeing more pure structural features.
- 3) We propose a cross-modal mamba fusion module (CMM) driven by a cross-modal interlaced scanning mechanism. This mechanism facilitates deep inter-modal feature interaction and global context extraction, significantly enhancing the perception and fusion of complementary cross-modal features.
- 4) We conduct extensive training and testing using state-of-the-art object detection methods on the DSEC-Det and PKU-DAVIS-SOD datasets, demonstrating that our proposed MCFNet significantly surpasses existing approaches in performance.

## 2 Related work

This section first introduces existing object detection algorithms in dynamic traffic scenarios and then introduces the working principle of event cameras and event representation methods.

### 2.1 Object detection in dynamic traffic scenarios

**RGB & RGB-radar fusion.** Wang et al. (2024) proposed the Mamba YOLO detector, which enhances the local modeling capabilities of state-space models (SSMs) in traffic object detection by introducing a residual gating (RG) mechanism. This detector utilizes selective two-dimensional (2D) scanning to process high-resolution image features, achieving competitive performance with linear computational complexity. YOLOv11 further improves traffic object detection by enhancing feature extraction and adopting a lightweight design, delivering both high precision and low latency. These improvements enable rapid responses and support safe decision-making in autonomous driving scenarios (Khanam and Hussain, 2024). Although image-based object detection methods provide excellent real-time performance, RGB cameras are susceptible to performance degradation under adverse weather or varying lighting conditions, which can lead to detection failures (Liu et al., 2020, 2021, 2024a). To address this limitation, some researchers have introduced radar sensors, which are immune to lighting variations, and proposed their fusion with RGB images to enhance perception robustness in low-light or dynamically lit environments. For example, Li et al. (2024) developed RCTrans, a radar-camera fusion model based on Transformers. It enhances sparse radar point cloud features using a dense radar encoder and progressively localizes targets via a pruning order decoder. Similarly, Wang et al. (2023) integrated image and point cloud data to design a module that combines occlusion state estimation with optimal appearance feature selection, effectively mitigating occlusion-related challenges in traffic object tracking for autonomous vehicles. However, radar's relatively low scanning frequency (typically 10–20 Hz) can lead to motion information loss or distortion in high-speed scenarios, potentially compromising detection accuracy and threatening the safe and stable operation of autonomous driving systems (Liu et al., 2023b).

**RGB-event fusion.** Neuromorphic cameras have recently been introduced to overcome the limitations of RGB cameras and radar in capturing motion information. Due to their asynchronous output,

event cameras offer exceptionally high temporal resolution and a wide dynamic range, enabling robust performance in complex and dynamic traffic environments. In the context of object detection using fused RGB and event data, existing approaches can be broadly classified into two categories: late fusion and intermediate fusion. Late fusion methods operate at the decision level. For example, Chen (2018) applied non-maximum suppression (NMS) to merge detection outputs from both modalities; Li et al. (2019) employ dempster-shafer theory to integrate events and frames for vehicle and pedestrian detection; and the related study (Jiang et al., 2019) proposed combining confidence maps derived from each modality. However, these approaches typically suffer from insufficient feature interaction and fail to fully leverage the complementary properties of RGB and event data. In contrast, intermediate fusion strategies perform integration at the feature level. Tomy et al. (2022) adopt a straightforward concatenation of event and frame-based features to enhance performance; SFNet introduces two dedicated sub-modules to refine features from each modality for effective cross-modal fusion (Liu et al., 2024b); RENet designs a bidirectional fusion module to capture multi-modal features across spatial and channel dimensions (Zhou et al., 2023); SODformer proposes an asynchronous attention-based fusion mechanism (Li et al., 2023); and EOLO incorporates a symmetric fusion module with attention mechanisms to align RGB and event features (Cao et al., 2024b). EvImHandNet (Jiang et al., 2024) leverages the complementary advantages of event and RGB cameras for 3 dimensional (3D) hand mesh reconstruction through a fusion module that employs spatial attention mechanisms and fully connected layers for weighted fusion. However, it still suffers from limited cross-modal interaction. To address this issue and enhance cross-modal feature integration, CAFR (Cao et al., 2024a) introduces a self-attention-based fusion module that separately computes `rgb_cross_attention` and `event_cross_attention`. This dual-path design introduces parameter redundancy, resulting in increased computational overhead. Despite their advantages, these methods predominantly emphasize inter-modal feature interactions while neglecting the joint modeling of global contextual information from both modalities. This oversight limits the network's ability to adaptively exploit dynamic cues from event data and rich textures from RGB images in accordance with varying scene characteristics.

Furthermore, most fusion methods assume that both modalities share the same spatial resolution. However, widely used sensors such as asynchronous time-based image sensors (ATISs) and dynamic and

active pixel vision sensors (DAVISs), which output both event streams and intensity images at shared pixel locations, offer relatively low resolution and cannot meet the demands of traffic perception tasks. More commonly, modern imaging systems spatially separate RGB and event cameras, enabling the acquisition of high-resolution RGB images alongside event data. When conducting multimodal fusion on such data, resolution inconsistency must be addressed. Existing solutions often downsample the RGB images to match the resolution of event data, which results in a loss of high-frequency visual information and degraded perception performance. To mitigate this, we propose performing dynamic upsampling of event features prior to fusion, thereby maximizing the use of rich visual content and enhancing fusion effectiveness.

## 2.2 Event representation

The event camera is a neuromorphic sensor whose photosensitive chips consist of multiple independently operating comparators that generate events by detecting changes in light intensity (Gallego et al., 2020). Specifically, when a comparator at a pixel location perceives a brightness change and the voltage variation exceeds a preset threshold  $C$ , it generates an event  $e_k$ , which includes the position  $u = (x, y)$ , timestamp  $t_k$ , and polarity  $p_k$ . The process is as

$$\Delta L(u, t_k) = L(u, t_k) - L(u, t_k - \Delta t_k) = P_k C \quad (1)$$

where  $P_k \in \{-1, 1\}$  denotes the polarity of the event, and the values 1 and  $-1$  indicate an increase or decrease in intensity at the pixel, respectively;  $L(u, t_k)$  and  $L(u, t_k - \Delta t_k)$  denote the illumination intensity at time  $t$  and  $t - \Delta t$ , respectively.

Effectively representing event data is crucial for accurate modeling. Existing fusion frameworks often convert asynchronous events into dense, image-like representations to enable the use of mature machine learning algorithms and neural network architectures. These dense representations can be broadly classified into four categories: image-based methods (Maqueda et al., 2018; Zhu et al., 2018a), timestamp-based methods (Kim et al., 2021; Park et al., 2016), voxel-based methods (Zhu et al., 2018b), and motion compensation methods (Gallego et al., 2018; Gu et al., 2021; Paredes-Vallés et al., 2021, 2023; Shiba

et al., 2022). Image-based methods typically rely on event statistics or polarity counting, which often leads to a significant loss of temporal information. Timestamp-based methods, such as Time Surface (Lagorce et al., 2016), HATS (Sironi et al., 2018), and DiST (Kim et al., 2021), apply temporal decay within event windows, assigning higher weights to more recent events. Voxel-based methods, like Voxel Grid (Zhu et al., 2018b), divide raw event streams into temporal bins and apply interpolation techniques to build voxelized representations. However, these methods are highly susceptible to thermal noise and dark current noise, which can degrade the quality of subsequent structural information extraction.

Recent motion compensation approaches (Gallego et al., 2018; Gu et al., 2021; Shiba et al., 2022; Paredes-Vallés et al., 2021, 2023; Wan et al., 2024) have shown promising results and can be categorized into model-based, self-supervised, and supervised learning methods. Model-based techniques (Gallego et al., 2018; Gu et al., 2021; Shiba et al., 2022) simulate motion and optimize models based on contrast maximization. Self-supervised methods typically estimate optical flow by assuming brightness constancy and linear motion, which are often violated in real-world conditions involving complex motion or varying lighting (e.g., vehicle headlights and streetlights), leading to artifacts and noise in reconstructed frames. To overcome these limitations, some studies (Paredes-Vallés et al., 2021, 2023) incorporate recurrent structures to enhance temporal modeling and mitigate the shortcomings of overly simplistic assumptions. However, these methods often increase the training complexity, and their task-decoupled design limits the optical flow network's ability to model complex motion in semantically rich scenes. Supervised methods, on the other hand, require ground truth optical flow, which is often lacking in most object detection datasets and impractical for real-world applications, thus not discussed here.

### 3 Proposed method

This section first introduces the principle of Mamba in Section 3.1, then describes the overall architecture of the proposed method in Section 3.2. Section 3.3 introduces the detailed information of the ECM, revealing its internal working principles. Section 3.4 presents the design of the EDUM. Finally, Section 3.5 introduces the CMM.

### 3.1 Introduction of SSMs and mamba

Mamba represents a novel sequence modeling architecture, fundamentally based on selective SSMs (Gu and Dao, 2023). SSM is a linear model designed to characterize the dynamic behavior of systems over time, mapping 1 dimensional (1D) input signals  $x(t) \in R$  to  $N$ -dimensional latent states  $h(t) \in R^N$ , before projecting them back to 1D output signals  $y(t)$ . The mathematical formulation is expressed as

$$\begin{cases} h'(t) = Ah(t) + Bx(t) \\ y(t) = Ch(t) + Dx(t) \end{cases} \quad (2)$$

where  $A \in R^{N \times N}$  is the state transition matrix,  $B \in R^{N \times 1}$  is the mapping matrix from input to state,  $C \in R^{N \times 1}$  is the state-to-output matrix, and  $D \in R$  is the input-to-output parameter.

Mamba introduces the selective state space scanning (S6) mechanism, which incorporates a learnable time-scale parameter  $\Delta$  that dynamically adapts to the input (Gu and Dao, 2023). This design overcomes the linear time-invariant (LTI) limitation of traditional SSMs and enhances global modeling capability. Specifically,  $\Delta$  controls the discrete-time dynamics by scaling the state transition at each input position, enabling the model to adjust how quickly or slowly it updates its internal state. As a result, the model can respond rapidly to abrupt changes with smaller  $\Delta$ , or integrate information over longer contexts with larger  $\Delta$ , achieving fine-grained control over temporal resolution. The model is discretized using a zero-order hold (ZOH), as detailed below:

$$\bar{A} = \exp(\Delta A), \quad \bar{B} = (\Delta A)^{-1}(\exp(\Delta A) - I)\Delta B \quad (3)$$

$$h_t = \bar{A}h_{t-1} + \bar{B}x_t, \quad y_t = Ch_t + Dx_t \quad (4)$$

where  $\Delta A$  and  $\Delta B$  represent the product of matrices  $A$  and  $B$  respectively with the scalar  $\Delta$ , which plays the role of scaling continuous-time state changes and inputs;  $\bar{A}$  is the discrete state transfer matrix,  $\bar{B}$  is the discretized input matrix, and  $I$  is the identity matrix. In Eq. (2),  $h_t$  denotes the hidden state at discrete time step  $t$ , and  $x_t, y_t$  are the input and output, respectively. Our proposed CMM module is built upon this mamba architecture.

### 3.2 Overview of MCFNet

In this section, we present the motion cue fusion network (MCFNet), as illustrated in Fig. 2, which takes RGB images and corresponding event streams as inputs, and achieve precise pixel-level spatiotemporal alignment and adaptive feature fusion across modalities. As shown in Fig. 2, the ECM estimates optical flow fields to temporally align event streams through warping operations, generating high-quality event representations tailored for detection. Subsequently, two parallel branches are used for modality-specific feature extraction, independently processing RGB images and event frames. Each branch adopts the CSPDarkNet backbone from the YOLOX framework (Ge et al., 2021), producing multi-scale feature maps. To address the resolution mismatch between RGB and event sensors in modern imaging systems, we introduce the EDUM, which adaptively refines upsampling kernels based on the spatial distribution of event features. This design facilitates the generation of high-resolution, high-fidelity event representations. Next, the CMM fusion module fuses features from both modalities at three hierarchical levels, adaptively integrating complementary information while preserving global contextual cues. Finally, the fused multi-scale features are processed by the FPN+PANet framework (Lin et al., 2017; Liu et al., 2018), followed by a detection head based on YOLOX for object classification and bounding box regression.

### 3.3 Event correction module

Due to the difference in temporal resolution between RGB and event cameras, there exists a temporal misalignment between the two modalities, which adversely affects precise cross-modal fusion and the extraction of discriminative features. To address this issue, motion compensation methods estimate the optical flow of the event stream to map events to the timestamp of the corresponding RGB frame, thereby achieving temporal alignment across modalities. However, these methods rely on assumptions of illumination consistency and linear motion, which are often violated in highly dynamic traffic scenarios, leading to inaccurate optical flow estimation and temporal alignment. To overcome the limitations, we propose an end-to-end architecture that integrates an optical flow-based ECM with an object detection network. This architecture facilitates the joint optimization of optical flow estimation and object detection

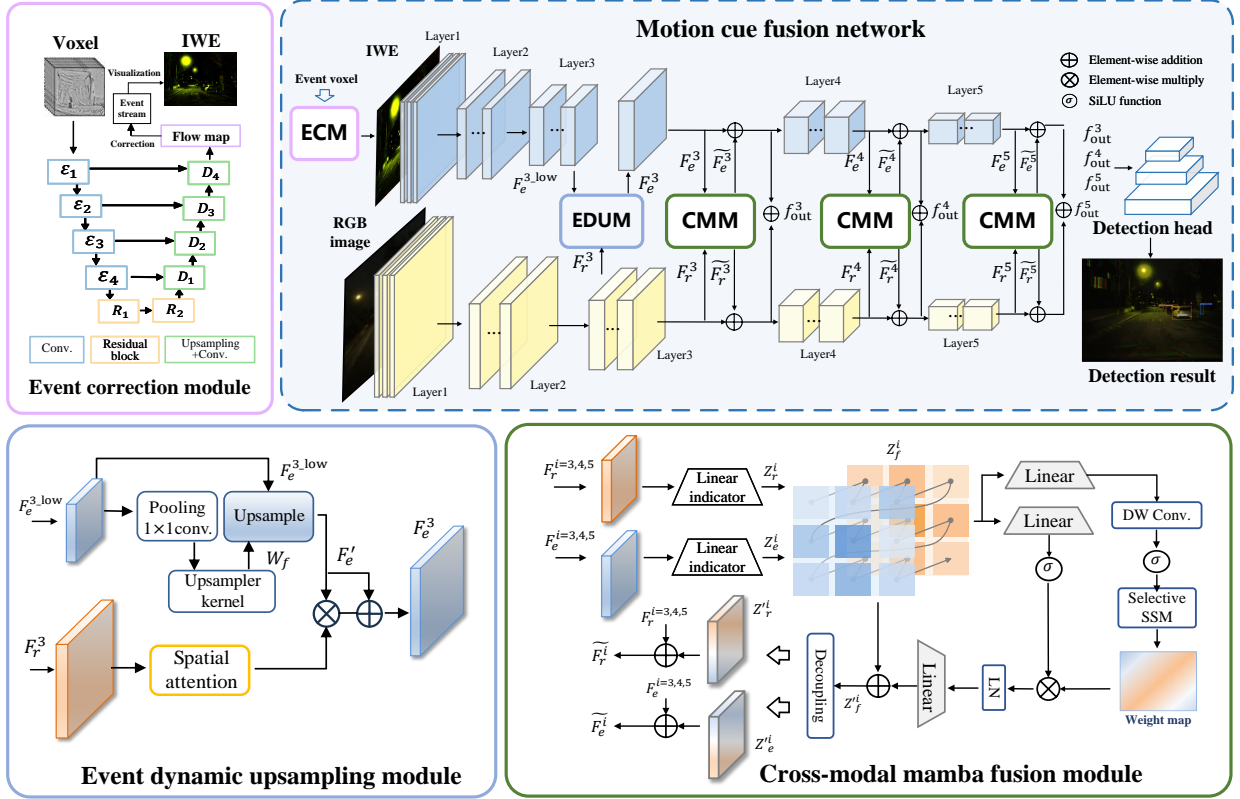


**Fig. 2** Pipeline of the proposed motion cue fusion network (MCFNet) is as follows. Voxels generated from raw event streams are first processed by the event correction module (ECM; see Section 3.3) to produce high-quality event frames. These frames, along with RGB images, are then fed into two separate CSPDarkNets for modality-specific feature extraction. The event dynamic upsampling module (EDUM; see Section 3.4) takes the features from the stage-3 layer to align the spatial resolutions of both modalities. This is followed by the cross-modal mamba fusion module (CMM; see Section 3.5) to perform cross-modal fusion. FPN combined with PANet further integrates multi-scale features, and finally, the decoder outputs category and bounding box predictions for each detected object.

tasks. By feeding the output of the ECM into the detection network and utilizing a unified backpropagation mechanism, the object detection supervisory signals can directly guide the learning of optical flow, thereby enabling the model to capture scene features that go beyond conventional assumptions of constant illumination and linear motion. As a result, the generated event representations are better tailored to the requirements of object detection.

Specifically, we extract the event stream  $e = (x_k, y_k, t_k, p_k)k = 1^N$  between the exposures of two consecutive image frames, where  $t_0 < t_k < t_0 + \Delta t$ , and to be consistent with the RGB sampling interval,  $\Delta t$  is set to 50 ms to define the temporal window. To convert the unstructured event stream into a tensor form acceptable to the network, we adopt a voxel-based event representation method (Zhu et al., 2018b). Specifically, we map the event stream  $e$  into a three-dimensional voxel grid  $E \in \mathbb{R}^{B \times H \times W}$ , where  $B$  is

the number of temporal bins. Following the setting in [Zhu et al. \(2018b\)](#), we set  $B = 5$ . The events are assigned to bins based on their timestamps, and we first normalize the event timestamps accordingly:

$$t_k^* = \frac{t_k - t_0}{t_{-1} - t_0}, t_k^* \in [0, 1] \quad (5)$$

where  $t_0$  and  $t_{-1}$  represent the timestamps of the first and last events in the current event sequence, respectively. For each partition, each event (indexed as  $k$ ) is assigned its polarity  $p_k$  to the two nearest time bins according to the following formula, with the weights determined by the triangular kernel function:

$$E(x_k, y_k, t) = \sum_k p_i \times \kappa(t - t_k^*(B - 1)), \kappa(a) = \max(0, 1 - |a|) \quad (6)$$

ECM predicts horizontal and vertical optical flow for each pixel within the interval and warps the events to align with a reference timestamp  $t_{\text{ref}}$ , achieving temporal alignment across modalities:

$$\begin{aligned} x'_k &= x_k + (t_{\text{ref}} - t_k) \times u(x_k, y_k) \\ y'_k &= y_k + (t_{\text{ref}} - t_k) \times v(x_k, y_k) \end{aligned} \quad (7)$$

We then apply bilinear interpolation to the compensated event stream  $e' = (x'_k, y'_k, t_k, p_k)_{k=1}^N$  to map events to their nearest pixel locations, using the surrounding four neighbors and performing a weighted sum based on polarity and visualize it, finally obtaining the Image of Warping Event (IWE)  $\in \mathbb{R}^{H \times W \times 3}$ :

$$\text{IWE} = \sum_k p_k \cdot \max(0, 1 - |e'_k(x, y) - e_k(x, y)|) \quad (8)$$

**Loss function.** In ECM, we choose to train in a self-supervised manner and use a contrast maximization framework loss for motion compensation. Following the approach in [Ye et al. \(2020\)](#), we use bilinear interpolation to generate an average timestamp image for each pixel under each polarity  $p'$ . And we optimize the loss function by minimizing the sum of squared differences between the forward- and

backward-warped event images:

$$T_p^*(x; (u, v) | t_{\text{ref}}) = \frac{\sum_j \kappa(x - x'_j) \kappa(y - y'_j) t_j^*}{\sum_j \kappa(x - x'_j) \kappa(y - y'_j) + \epsilon} \quad (9)$$

$$j = \{i \mid p_i = p'\}, \quad p' \in \{+, -\}, \quad \epsilon \rightarrow 0$$

where  $(u, v)$  is the estimated optical flow,  $(x'_j, y'_j)$  are the warped event coordinates,  $t_j^*$  is the normalized timestamp, and  $\kappa(\cdot)$  denotes the bilinear interpolation kernel. The contrast loss is then defined as

$$\mathcal{L}_{\text{contrast}}(t_{\text{ref}}^*) = \sum_x [T_+(x; (u, v) | t_{\text{ref}}^*)^2 + T_-(x; (u, v) | t_{\text{ref}}^*)^2] \quad (10)$$

$$\mathcal{L}_{\text{contrast}} = \mathcal{L}_{\text{contrast}}(1) + \mathcal{L}_{\text{contrast}}(0)$$

To regularize the optical flow estimation, we introduce a smoothness loss that penalizes discontinuities in the flow field (Zhu et al., 2018a). For each pixel  $(x, y)$ , its neighbors are denoted by  $\mathcal{N}(x, y)$ , and the robust Charbonnier penalty function  $\rho(\cdot)$  is applied to flow gradients:

$$l_{\text{smoothness}} = \sum_{x, y} \sum_{i, j \in \mathcal{N}(x, y)} \rho(u(x, y) - u(i, j)) + \rho(v(x, y) - v(i, j)) \quad (11)$$

$$\rho(x) = \sqrt{x^2 + \epsilon^2}$$

The total loss is a weighted sum of contrast loss and smoothness loss:

$$\mathcal{L}_{\text{ECM}} = \mathcal{L}_{\text{contrast}} + \lambda_1 \mathcal{L}_{\text{smooth}} \quad (12)$$

**Training strategy.** Benefiting from the fast convergence and strong generalization ability of ECM, we first jointly train the network on a representative subset of the DSEC-Det dataset. The trained model is then used to generate deterministic IWEs for the entire dataset, which serve as input to train the object detection component of MCFNet. This strategy ensures high detection performance while significantly reducing training costs. To initialize the network, we use the official pre-trained weights from Zhu et al. (2018a) and Ge et al. (2021).

### 3.4 Event dynamic upsampling module

Due to differences in resolution and field of view between RGB and event cameras, their outputs exhibit spatial misalignment. To compensate for this spatial discrepancy, existing fusion methods often downsample RGB frames to match the resolution of event data at the input stage (Liu et al., 2024b; Tomy et al., 2022; Zhou et al., 2023), which inevitably leads to the loss of high-frequency details and compression of informative content in RGB images, ultimately degrading perception performance. To address this issue, we propose the EDUM, which upsamples event features prior to modal fusion to fully exploit high-quality RGB information. However, conventional upsampling approaches typically rely on fixed-parameter transposed convolutions to enhance spatial resolution, ignoring variations in pixel distributions across different scenes. This often results in blurred details or visual artifacts. In contrast, our EDUM adaptively modulates upsampling weights based on the input features, allowing for more fine-grained and context-aware resolution enhancement.

Specifically, EDUM first applies global average pooling to the input event features  $F_e^{3,\text{low}} \in R^{B \times C \times H \times W}$  and implements sequential interaction through  $1 \times 1$  convolution. The learned weights are then assigned to the transposed convolution kernel  $W \in R^{B \times C_{\text{in}} \times C_{\text{out}} \times 3 \times 3}$  to perform transposed convolution upsampling on low-resolution Event features, yielding high-resolution Event features  $F'_e \in R^{B \times C \times 2H \times 2W}$ . The formulation is as

$$D = \text{GAP}(F_e^{3,\text{low}}) \quad (13)$$

$$W_f = W \otimes \text{Conv}_{1 \times 1}(D) \quad (14)$$

$$F'_e = \text{DeConv}(W_f, F_e^{3,\text{low}}) \quad (15)$$

where  $\text{GAP}$  represents the global average pooling and  $\text{DeConv}$  represents the de-convolution operation.

Simultaneously, considering that event cameras inevitably generate noise due to their sensitivity to dark current and photocurrent, we leverage spatial attention maps derived from high-resolution RGB features of the third layer of the backbone network  $F_r^3 \in R^{B \times C \times 2H \times 2W}$  to suppress noise amplification during upsampling. We exploit the smoothness of RGB features to enhance the up-sampled event features,

ultimately obtaining enhanced high-resolution event features  $F_e^3 \in R^{B \times C \times 2H \times 2W}$ . The formulation is as

$$F_e^3 = F'_e + F'_e \otimes \sigma(\text{Concat}(\text{AveP}(F_r^3), \text{MaxP}(F_r^3))) \quad (16)$$

where AveP is an average pooling layer, MaxP is a max pooling layer, and  $\sigma$  is the sigmoid function.

### 3.5 Cross-modal mamba fusion module

To simultaneously perceive the most valuable complementary information during cross-modal interaction, and adaptively leverage Event dynamics or RGB texture features for complementary fusion based on scene characteristics, we design CMM with a cross-modal interlaced scanning mechanism. This mechanism simultaneously performs inter-modal feature interaction and captures global information, selectively preserving salient features while filtering redundant information.

Specifically, we choose to fuse the two modalities in the third, fourth, and fifth layers of the backbone network and input the fused features into FPN+PANet. Therefore, we first project the two input modality features of CMM,  $F_e^{i=3,4,5} \in R^{C \times H \times W}$  and  $F_r^{i=3,4,5} \in R^{C \times H \times W}$ , to the latent space through a linear transformation, where  $i$  represents the feature from the  $i$ -th layer of the backbone network. The magnitude and offset of modal features are then adjusted through scaling factors to accommodate different modal feature distributions, enabling feature domain alignment and distribution normalization across different modalities.

$$\begin{cases} Z_e^i = F_e^i \odot r_e^i + \beta_e^i \\ Z_r^i = F_r^i \odot r_r^i + \beta_r^i \end{cases} \quad (17)$$

where  $r_e^i/r_r^i$  and  $\beta_e^i/\beta_r^i$  represent the scaling and offset factors respectively, and  $\odot$  denotes the element-wise multiplication operation.

Subsequently,  $Z_e^i$  and  $Z_r^i$  are concatenated along the  $W$  dimension to obtain the feature-level fine-grained fusion features  $Z_f^i \in \mathbb{R}^{C \times H \times 2W}$ . This concatenation operation provides the spatial and structural foundation for fusion, enabling the interaction of information from both modalities within a

unified representation space.

$$Z_f^i = \text{Cross\_concat}(Z_e^i, Z_r^i, \text{dim} = W) \quad (18)$$

The mixed features  $Z_f^i$  are flattened along the  $H$  and  $W$  dimensions and then fed into the *SSMs*, allowing each modality to selectively extract relevant features based on information from the other. Through global spatial interactions between the two modalities, a *WeightMap* is generated to reflect their complementary relationship, guiding the adaptive utilization of either the dynamic properties of events or the rich semantic features of RGB. Additionally, the integration of depth-wise separable convolution (DWConv) and Layer Normalization further improves computational efficiency while enhancing the capability to model cross-modal correlations. As a result, enhanced mixed features  $Z_f'^i$  are generated.

The formulation is as

$$\text{WeightMap} = \text{SSM}(\bar{A}, \bar{B}, C)(Z_f'^i) \quad (19)$$

$$Z_f'^i = \text{LN}(\text{Liner}(\text{WeightMap} \odot Z_f)) \quad (20)$$

where  $\bar{A}$ ,  $\bar{B}$ , and  $C$  are defined in Eqs. (2) and (3), and represent the discretized state transition matrix, the input-to-state mapping matrix, and the state-to-output matrix, respectively. Finally, the feature  $Z_f'^i$  is decoupled back to the two modalities, generating enhanced modal features  $Z_e'^i$  and  $Z_r'^i$ , which are then fused with the original features  $Z_e^i$  and  $Z_r^i$  through residual connections to obtain  $\widetilde{F}_e^i$  and  $\widetilde{F}_r^i$ , respectively. This approach effectively enhances modality complementarity while preserving the original feature information. The formulation is as

$$Z_e'^i, Z_r'^i = \text{decouple}(Z_f'^i) \quad (21)$$

$$\widetilde{F}_e^i = F_e^i + Z_e'^i \quad (22)$$

$$\widetilde{F}_r^i = F_r^i + Z_r'^i \quad (23)$$

We then add and fuse the adaptively enhanced features from the two modalities to obtain  $f_{\text{out}}^i$ , which

is subsequently fed into the FPN+PANet for multi-scale semantic enhancement and feature integration.

## 4 Experiments

This section first describes the used dataset as well as the experimental settings. Subsequently, quantitative and qualitative results are presented to demonstrate the effectiveness of our method. Finally, we perform an ablation study for each module in our network.

### 4.1 Datasets and experimental settings

In the experiments, we verify the effectiveness of our model on two real scene datasets, namely DSEC-Det (Gehrig et al., 2021) and PKU-DAVIS-SOD (Li et al., 2023).

**DSEC-Det.** The dataset contains wide-baseline stereo data captured using an RGB camera ( $1440 \times 1080$ ) and a high-resolution monochrome event camera ( $640 \times 480$ ). It comprises 53 sequences, with 39 used for training and 14 for testing, totaling  $6.39 \times 10^4$  frames (Gehrig et al., 2021).

The DSEC-Det dataset has multiple versions of annotations. Among them, the automatic annotation methods used by DAGr (Gehrig and Scaramuzza, 2024) and FPN-fusion (Tomy et al., 2022) lead to degraded labeling quality, while SFNet (Liu et al., 2024b) provides manually annotated labels that are more comprehensive and accurate. For this reason, we adopt the annotation information from SFNet (Liu et al., 2024b), and follow their data split strategy to maintain fair comparisons.

**PKU-DAVIS-SOD.** The PKU-DAVIS-SOD dataset collected by the DAVIS346 event camera provides spatially aligned RGB frame and event stream ( $346 \times 260$ ) data, with  $6.713 \times 10^5$  labels for training and  $2.141 \times 10^5$  for testing. Each subset is further divided into three typical scenes (normal, motion blur, and low-light) (Li et al., 2023).

**Implementation details.** We train the MCFNet using the Adam optimizer with a learning rate of  $5 \times 10^{-4}$  and a batch size of 2. The network architecture incorporated CSPDarkNet from YOLOX (Ge et al., 2021) as both the RGB backbone and Event backbone. The training pipeline implemented standard YOLO data augmentation methods for RGB input, including mosaic and mixup techniques.

Due to the inconsistent resolution of the two modalities in the two datasets, different configurations

are adopted. For experiments on the PKU-DAVIS-SOD dataset, where RGB and Event data share the same resolution, our method is implemented without the EDUM module. In comparative experiments, since EvImHandNet (Jiang et al., 2024) is originally designed for hand mesh reconstruction, we only replace our CMM with its fusion module CFM for fair comparison while retaining all other architectural components. For other methods, we follow their original training strategies to ensure a fair comparison.

**Evaluation metrics.** We adopt COCO metrics (Lin et al., 2014) to evaluate the accuracy of object detection, including mAP50 with an IOU threshold of 50% and mAP, which averages over IOUs between 50% and 95%. To assess model efficiency, we also report parameters, FLOPs, and runtime.

## 4.2 Quantitative results

To evaluate the superiority of our approach, we compare MCFNet with state-of-the-art (SOTA) object detection methods. Furthermore, to validate the effectiveness of our event representation strategy, we conduct comparative experiments against leading event representation and motion compensation techniques.

**Comparison with SOTA object detection methods.** We compare our method with recent SOTA object detection methods, including two event-based methods: RVT (Gehrig and Scaramuzza, 2023) and SAST (Peng et al., 2024); three RGB-based methods: YOLOv11 (Khanam and Hussain, 2024), YOLOv12 (Tian et al., 2025) and Mamba-YOLO (Wang et al., 2024); and four fusion-based methods: FPN-fusion (Tomy et al., 2022), SODFormer (Li et al., 2023), EOLO (Cao et al., 2024b), and SFNet (Liu et al., 2024b). In addition, to compare with other fusion methods, we replace our CMM with the CNN-based fusion method CFM in EvImHandNet (Jiang et al., 2024) and the transformer-based fusion module in CAFR (Cao et al., 2024a).

As shown in Table 1, our MCFNet outperforms existing object detection methods on both datasets. Specifically, on the class-imbalanced DSEC-Det dataset, our method outperforms the second-best method by 1.7% and 7.4% in mAP and mAP50, respectively. On the class-balanced DSEC-Det dataset, our method shows consistent superiority, with mAP and mAP50 improved by 1.7% and 3.3%, respectively. Furthermore, when comparing different methods, although our MCFNet achieves leading performance in detection accuracy, it incurs a higher computational cost, with 227.8 G FLOPs and an inference time

of 47.3 ms, compared to lightweight unimodal models such as Mamba-YOLO (49.6G) (Wang et al., 2024) and YOLOv11 (35.7 ms) (Khanam and Hussain, 2024). Nevertheless, MCFNet maintains high accuracy while achieving an inference speed of approximately 21 FPS, demonstrating preliminary real-time processing capability. Furthermore, compared to other multimodal methods (e.g., SFNet, which has a similar inference time of 44.8 ms but significantly lower accuracy), our approach presents a favorable balance between performance and efficiency.

**Table 1** Performance comparison of SOTA object detection methods under different datasets (mAP50/ mAP). The best and the second-best performances are marked in red bold and blue bold, respectively. Note: M denotes million parameters.

	Method	Pub. & Year	DSEC-Det			PKU-DAVIS-SOD			Parameter	
			Class-balanced mAP50/mAP	Class-imbalanced mAP50/mAP	FLOPs	Runtime	mAP50/ mAP	FLOPs		
RGB	YOLOv11	arXiv'24	84.5/ <b>59.2</b>	<b>59.1/40.1</b>	102.3 G	35.7 ms	58.0/30.9	44.2 G	15.6 ms	20.1 M
	Mamba-YOLO	AAAI'25	83.4/55.6	53.9/34.7	49.6 G	58.7 ms	57.1/29.8	21.6 G	21.0 ms	21.8 M
	YOLOv12	arXiv'25	86.8/58.8	55.0/34.6	90.1 G	46.5 ms	60.2/32.4	12.22 G	13.4 ms	19.6 M
Event	RVT	CVPR'23	51.1/26.6	25.1/12.9	19.6 G	11.9 ms	50.3/25.6	6.5 G	7.1 ms	18.5 M
	SAST	CVPR'24	53.8/39.3	24.3/12.1	18.5 G	18.8 ms	<b>48.7/24.5</b>	6.2 G	16.7 ms	18.5 M
RGB-Event	FPN-fusion	ICRA'22	56.8/30.7	36.9/19.7	89.6 G	30.8 ms	36.6/19.5	49.7 G	24.0 ms	65.6 M
	SODFormer	TPAMI'22	—	—	—	—	50.4/20.7	62.5 G	39.7 ms	82.0 M
	EOLO	ICRA'24	65.1/37.8	33.9/19.6	13.7 G	330.2 ms	47.2/22.0	8.9 G	326.4 ms	21.5 M
	SFNet	ITS'24	80.0/50.9	51.4/30.4	209 G	44.8 ms	59.6/31.9	135.9 G	42.3 ms	57.5 M
	Our pipeline + CFM	CVPR'24	86.4/53.1	<b>60.0/35.3</b>	256.0 G	58.9 ms	60.0/30.8	80.93 G	17.2 ms	46.0 M
	Our pipeline + CAFR	ECCV'24	<b>87.4</b> /54.8	59.9/34.6	208.5 G	50.4 ms	<b>61.2/31.8</b>	66.51 G	18.9 ms	43.6 M
	MCFNet (this study)	—	<b>90.7/60.9</b>	<b>67.4/41.8</b>	227.8 G	47.3 ms	<b>61.8/32.6</b>	72.68 G	18.8 ms	52.1 M

In addition, on the PKU-DAVIS-SOD dataset, our method outperforms the SODFormer (Li et al., 2023) by 11.9% and 11.4% in mAP and mAP50, respectively. As shown in Table 2, our model shows consistent performance advantages under various challenging conditions, outperforming SODFormer (Li et al., 2023) by 10.2%, 9.6%, and 11.8% in mAP50 for normal, low-light, and motion blur subsets, respectively. These results indicate that our method achieves more robust object detection performance by accurate spatiotemporal alignment and adaptive fusion across modalities, especially in challenging traffic scenes with complex lighting conditions and motion blur.

**Cross-scene evaluation on PKU-DAVIS-SOD.** To further demonstrate the robustness of our proposed method, we conduct a cross-scene validation. Specifically, we transferred a model trained solely on the DSEC-Det dataset to the PKU-DAVIS-SOD dataset. Due to the difference in the number of object

**Table 2** Performance comparison with SOTA method on different scene subsets of PKU-DAVIS-SOD dataset. The best and the second-best performances are marked in red bold and blue bold.

Method	Pub&Year	PKU-DAVIS-SOD					
		Normal		Motion_blur		Low_light	
		mAP	mAP50	mAP	mAP50	mAP	mAP50
SODFormer	TPAMI'22	24.1	56.9	18.3	43.2	12.2	37.4
SFNet	ITS'24	32.3	62.4	23.1	46.7	17.6	41.2
Our pipeline + CFM	CVPR'24	33.6	65.1	25.0	50.9	21.2	48.6
Our pipeline + CAFR	ECCV'24	<b>34.4</b>	<b>66.6</b>	<b>26.0</b>	<b>51.7</b>	<b>21.6</b>	<b>49.9</b>
MCFNet (this study)	—	<b>34.8+0.4</b>	<b>67.1+0.5</b>	<b>26.0</b>	<b>52.8+1.1</b>	<b>21.8+0.2</b>	<b>49.2-0.7</b>

categories between the two datasets, we applied only light fine-tuning to the detection head. As shown in Table 3, despite differences in data distribution and class definitions between datasets, our model still outperformed other methods, demonstrating strong generalization and robustness across domains.

**Table 3** Cross-scene performance comparison with SOTA methods on the PKU-DAVIS-SOD dataset. The best performance is marked with red bold.

Method	Pub&Year	PKU-DAVIS-SOD	
		mAP	mAP50
SFNet	ITS'24	19.7	41.9
Our pipeline + CFM	CVPR'24	18.5	39.5
MCFNet(this study)	—	<b>24.7</b>	<b>49.7</b>

**Comparison with SOTA event frame accumulation methods and motion compensation methods.** To further demonstrate the superiority of our ECM representation method, we compare it with four Event frame accumulation methods: Timestamp (Park et al., 2016), DiST (Kim et al., 2021), Voxel (Zhu et al., 2018b), and TAF (Liu et al., 2023a). Additionally, we evaluate five motion compensation methods: (i) model-based (MB): CMax (Gallego et al., 2018), ST-PPP (Gu et al., 2021) and MCM (Shiba et al., 2022), (ii) self-supervised learning (SSL): ConGru-EV-FlowNet (Paredes-Vallés et al., 2021, 2023) configuration with the best performance. For the motion compensation method, the resulting IWE is used as input for our detection network. We keep the detection network, upsampling module, and fusion module the same and only change the input of event modality. The results are reported in Table 4.

Among all event frame accumulation methods, our ECM achieves optimal performance by predicting motion vectors to align timestamps, resulting in accurate temporal alignment and high-quality frames with sharp edges and reduced noise. For example, on the class-imbalanced DSEC-Det dataset, our event representation outperforms voxel (Zhu et al., 2018b) by 1.7% on mAP50.

**Table 4** Performance comparison with state-of-the-art (SOTA) event representation methods and motion compensation methods. The best and second-best performances are marked in red bold and blue bold, respectively. MB: Model-based; SSL: Self-supervised learning.

	Method	Pub. & Year	Inference time	DSEC-Det (Class-balanced)		DSEC-Det (Class-imbalanced)		PKU-DAVIS-SOD	
				mAP	mAP50	mAP	mAP50	mAP	mAP50
MB	CMax	CVPR'18	2.42s	60.0	89.6	<b>41.5</b>	65.8	31.1	60.3
	ST-PPP	ICCV'21	2.48 s	<b>60.3</b>	89.9	41.4	<b>67.0</b>	31.2	60.2
	MCM	ECCV'22	65 s	60.1	<b>90.0</b>	41.3	66.0	31.5	60.0
SSL	ConvGRU-EV-FlowNet	NeurIPS'21	0.48 s	60.1	89.9	41.3	66.0	<b>32.4</b>	62.0
	Federico et al.	ICCV'23	0.29 s	60.2	89.9	40.1	63.8	<b>32.4</b>	<b>62.3</b>
	TAF	IEEE Trans. TIM'23	—	60.2	89.6	39.7	63.3	31.0	59.9
	Timestamp	ICIP'16	—	59.7	89.3	40.5	65.6	31.7	60.9
	Voxel	CVPR'19	—	59.4	89.0	41.1	65.7	30.8	59.6
	DiST	ICCV'21	—	60.0	89.9	<b>41.5</b>	65.6	31.4	60.7
	ECM(this study)	—	0.03 s	<b>60.9</b>	<b>90.7</b>	<b>41.8</b>	<b>67.4</b>	<b>32.6</b>	<b>61.8</b>

Compared to model-based and self-supervised motion compensation methods, our ECM also demonstrates superior performance. For instance, on the class-imbalanced DSEC-Det dataset, our event representation surpasses ConvGRU-EV-FlowNet (Paredes-Vallés et al., 2021) by 1.4% on mAP50. This proves that when jointly trained with detection networks in an end-to-end architecture, our ECM learns scene features that overcome the limitations of brightness constancy and linear motion assumptions, generating event representations that are better suited for various complex scenarios and beneficial for object detection tasks. In contrast, different motion states and frequent illumination changes adversely affect optical flow estimation, leading to artifacts and noise generation in IWE, which impacts detection performance, as shown in Fig. 3.

### 4.3 Qualitative results

**Comparison with SOTA detection methods.** We compare MCFNet with two leading SOTA methods Our pipeline+CFM (Jiang et al., 2024) and SFNet (Liu et al., 2024b). As shown in Fig. 4, the first three columns show scenes with non-uniform exposure, while columns 4 and 5 show low-light multi-object scenes, and the last column is a motion blur scene. Our method achieves superior robustness compared to existing SOTA approaches in complex illumination conditions through accurate spatiotemporal alignment across modalities and excellent adaptive complementary fusion by simultaneously perceiving global information from both modalities in the scene, thereby enabling successful detection.

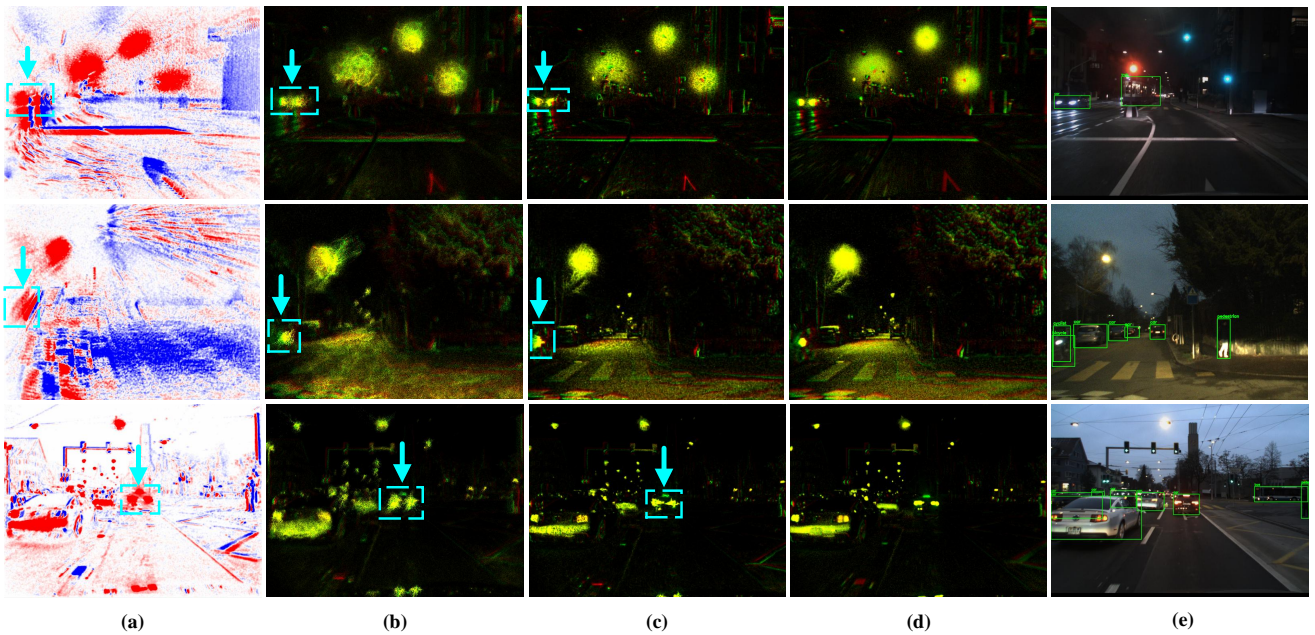


**Fig. 3** Qualitative comparison with SOTA motion compensation event representation methods on the DSEC-Det dataset: (a) ST-PPP, (b) ConvGRU-Ev-FlowNet, (c) Ev-FlowNet, (d) ECM(this study), and (e) GT.

**Comparison with SOTA event representation methods.** We compare our event representation generated from ECM with two leading SOTA motion compensation approaches ST-PPP, ConvGRU-EV-FlowNet (Gu et al., 2021; Paredes-Vallés et al., 2021) and representations generated by EvFlow without end-to-end joint training, as illustrated in Fig. 3. The first row shows a scenario of rapidly moving vehicles with bright self-emitting lights in nighttime conditions. The second row presents a scene where the ego vehicle's headlights illuminate the target vehicle while it simultaneously emits its own lighting during motion. In the third scenario, an examination of consecutive frames reveals that the center vehicle's brake lights have just activated in the current frame. These three scenarios collectively showcase environments with either rapid illumination variations or complex motion patterns. As illustrated in columns 2–4 of Fig. 3, existing motion compensation methods often fail under such conditions as environmental changes violate their underlying assumptions of brightness constancy and linear motion, resulting in artifacts, noise, and target deformation. In contrast, our ECM-generated representations maintain target fidelity while leveraging event motion characteristics, guided by the optimization from the object detection task.

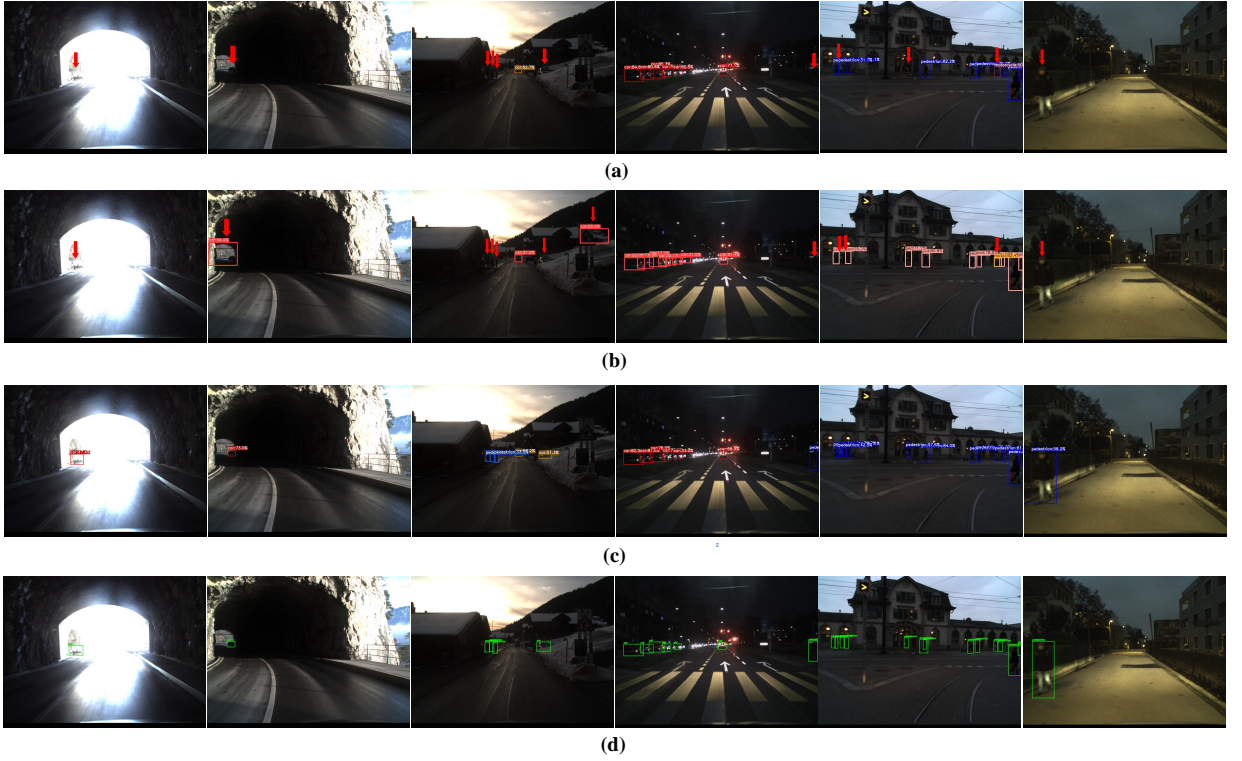


**Fig. 4** Qualitative comparison with two leading SOTA detection methods on the class-imbalanced DSEC-Det dataset: (a) EvImHnadNet; (b) SFNet; (c) MCFNet(this study); and (d) GT. We utilize red arrows to mark the failed cases.

#### 4.4 Ablation study

In this section, we present our ablation study results on the DSEC-Det dataset to validate the effectiveness of each component in our proposed MCFNet.

**Contribution of our MCFNet components.** We take dual-stream YOLOX architecture with Voxel Event representation and simple feature addition fusion as the baseline to perform a comprehensive ablation study and analyze the performance of each component in the MCFNet. Table 5 shows the results from different combinations of modules in our method. It can be observed that each proposed module contributes positively to the detection performance of MCFNet. Especially on the class-imbalanced DSEC-Det dataset, our model achieves significant improvements over the baseline, with increases of 8.1% and 12% in mAP and mAP50 metrics respectively, demonstrating the effectiveness of each module in dynamic traffic scenarios.

The feature maps before and after applying CMM are shown in Fig. 5. As observed in the first and second rows depicting nighttime scenes in Fig. 5, the event modality exhibits more stable imaging

**Table 5** Ablation study of proposed components. **Red bold** indicates improvement from baseline.

ECM	EDUM	CMM	DSEC-Det class-balanced		DSEC-Det class-imbalanced	
			mAP	mAP50	mAP	mAP50
YOLOX(voxel)	—	—	53.7	82.5	33.7	55.4
✓	—	—	53.8+0.1	82.7+0.2	34.1+0.4	55.6+0.2
✓	—	✓	55.9+2.2	85.9+3.4	34.0+0.3	56.9+1.5
✓	✓	—	60.0+6.3	89.4+6.9	40.4+6.7	64.7+9.3
✓	✓	✓	60.9+7.2	90.7+8.2	41.8+8.1	67.4+12.0

capabilities in low-light conditions compared to the RGB modality, due to its high dynamic range, enabling more effective target information capture. Conversely, in the daytime scenes shown in the third and fourth rows, when the ego vehicle moves simultaneously with target objects, events become sparse due to relative stasis or minimal relative motion. Meanwhile, RGB images under favorable lighting conditions contain rich chromatic, textural, and semantic information, facilitating more effective target capture. After CMM fusion, the model simultaneously models global information from both modalities to precisely identify inter-modal complementary relationships, selectively emphasizing key information through adaptive fusion to achieve complementary modal advantages and capture all target information in the scene.

**Benefits of joint training of ECM.** We validate the effectiveness of our joint training strategy on DSEC-Det (Gehrig et al., 2021). The two-stage training strategy refers to a configuration where the optical flow network parameters remain fixed without participating in the backpropagation process during detector training. Our ECM employs end-to-end joint network training, where event correction optimization is guided by detection results. As shown in the Table 6, our ECM learns scene features that surpass the assumptions of brightness constancy and linear motion, achieves more accurate temporal alignment, and generates event representations better aligned with object detection requirements, thereby delivering superior performance.

**Table 6** Comparing the results of EvFlowNet without joint training with ECM.

Method	Training strategy	DSEC-Det class-imbalanced	
		mAP	mAP50
EV-FlowNet	Two-stage	41.1	65.4
ECM (this study)	Joint training	41.8	67.4

**Selection of upsampling methods.** To validate the effectiveness of our dynamic upsampling method

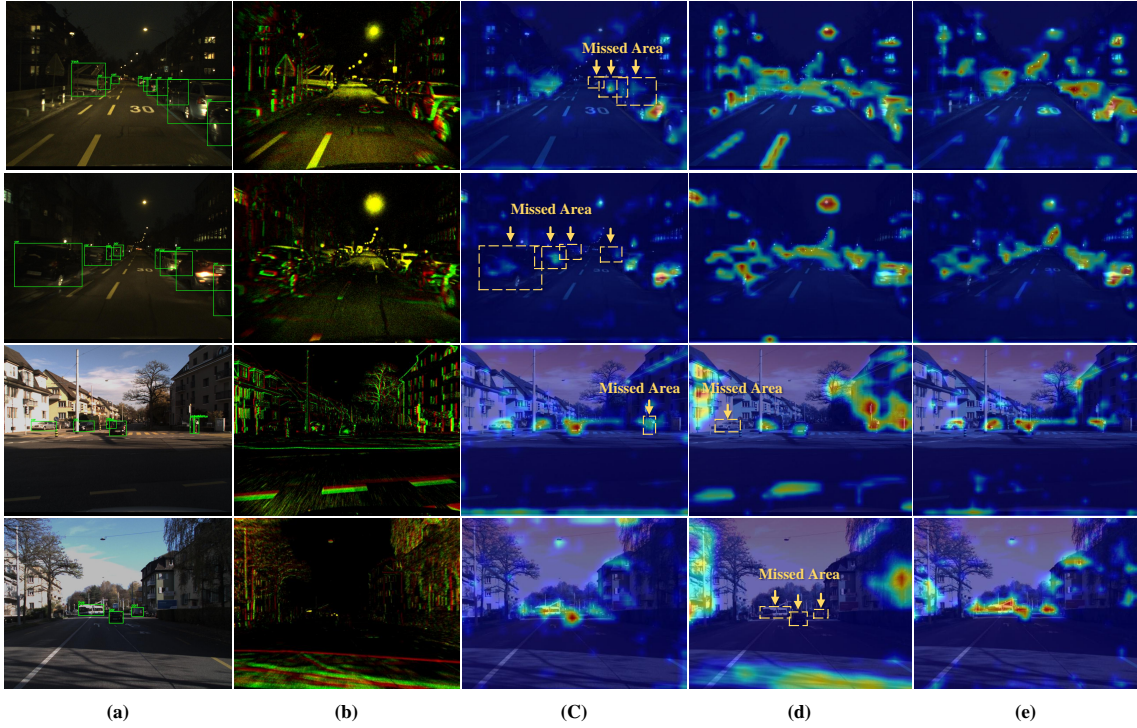


**Fig. 5** Visualization of features before and after CMM. (a) GT representing the scene, (b) Event representation corresponding to the scene, (c) feature visualization of RGB modality before it passes through CMM, (d) feature visualization of event modality before it passes through CMM, and (e) fused feature visualization after CMM module. The boxes indicate the unfocused target areas.

EDUM, we conducted comparative experiments against common upsampling approaches including Pixel Shuffle and transposed convolution. As demonstrated in Table 7, dynamically adjusting weights based on input enables the model to learn pixel distribution variations across different scenarios, thereby achieving more precise spatial alignment and enhanced detection performance.

**Table 7** Performance comparison of different upsampling methods.

Upsampling Method	DSEC-Det (class-imbalanced)	
	mAP	mAP50
Pixel Shuffle	40.7	65.2
Transposed conv ( $3 \times 3$ )	41.5	65.8
EDUM (this study)	41.8	67.4

## 5 Conclusion

In this study, we propose a Motion Cue Fusion Network (MCFNet) for robust object detection in dynamic traffic scenarios. ECM overcomes the limitations of the traditional assumptions of constant

illumination and linear motion in the optical flow estimation task by being effectively guided by the object detection task to obtain high-quality event frames. EDUM dynamically upsampling event features based on the feature space distribution, aligning the resolutions of the two modalities while maximizing the use of high-quality information. CMM enhances the accuracy of the model's perception and selection of dominant modal features in different scenarios by simultaneously performing inter-modal feature interaction and global information extraction, thereby achieving adaptive fusion. Experiments show that our MCFNet significantly outperforms existing methods in various complex and dynamic traffic scenarios.

Although the proposed method achieves excellent performance in detection accuracy, the introduction of spatiotemporal alignment for event data and the multimodal cross-fusion mechanism results in a relatively complex model structure with high computational overhead, posing challenges for deployment on resource-constrained devices. In future work, we plan to introduce sparsity constraints on event data. For example, using sparse token mechanisms to filter out inactive regions and perform fusion only where events occur, thereby reducing redundant computation. We also aim to explore dynamic token selection and model pruning to reduce computational load further and accelerate inference for real-time applications.

## References

Basha T., Moses Y., Kiryati N., 2013. Multi-view scene flow estimation: A view centered variational approach. *Int J Comput Vis*, **101**, 6–21.

Bayoudh K., Knani R., Hamdaoui F., Mtibaa A., 2022. A survey on deep multimodal learning for computer vision: advances, trends, applications, and datasets. *Vis Comput*, **38**, 2939–2970.

Berman S., Stern H., 2011. Sensors for gesture recognition systems. *IEEE Trans Syst Man Cybern Syst*, **42**, 277–290.

Brox T., Malik J., 2010. Large displacement optical flow: descriptor matching in variational motion estimation. *IEEE Trans Pattern Anal Mach Intell*, **33**, 500–513.

Cao H., Chen G., Xia J., Zhuang G., Knoll A., 2021. Fusion-based feature attention gate component for vehicle detection based on event camera. *IEEE Sens J*, **21**, 24540–24548.

Cao H., Zhang Z., Xia Y., Li X., Xia J., Chen G., et al., 2024a. Embracing events and frames with hierarchical feature refinement network for object detection. In: European Conference on Computer VisionSpringer, 161–177.

Cao J., Zheng X., Lyu Y., Wang J., Xu R., Wang L., 2024b. Chasing day and night: Towards robust and efficient all-day object detection guided by an event camera. In: 2024 IEEE International Conference on Robotics and Automation (ICRA), 9026–9032.

Chen K., Yu L., 2024. Motion deblur by learning residual from events. *IEEE Trans Multimed*, **26**, 6632–6647.

Chen N. F. Y., 2018. Pseudo-labels for supervised learning on dynamic vision sensor data, applied to object detection under ego-motion. In: 2018 IEEE/CVF Conference on Computer Vision and Pattern Recognition Workshops (CVPRW), 644–653.

Chen P., Guan W., Lu P., 2023. Esvio: Event-based stereo visual inertial odometry. *IEEE Robot Autom Lett*, **8**, 3661–3668.

Gallego G., Delbrück T., Orchard G., Bartolozzi C., Taba B., Censi A., et al., 2020. Event-based vision: A survey. *IEEE Trans Pattern Anal Mach Intell*, **44**, 154–180.

Gallego G., Rebecq H., Scaramuzza D., 2018. A unifying contrast maximization framework for event cameras, with applications to motion, depth, and optical flow estimation. In: Proceedings of the IEEE conference on computer vision and pattern recognition, 3867–3876.

Ge Z., Liu S., Wang F., Li Z., Sun J., 2021. YOLOX: Exceeding YOLO Series in 2021. <https://doi.org/10.48550/arXiv.2107.08430>.

Gehrig D., Scaramuzza D., 2024. Low-latency automotive vision with event cameras. *Nature*, **629**, 1034–1040.

Gehrig M., Aarents W., Gehrig D., Scaramuzza D., 2021. Dsec: A stereo event camera dataset for driving scenarios. *IEEE Robot Autom Lett*, **6**, 4947–4954.

Gehrig M., Scaramuzza D., 2023. Recurrent vision transformers for object detection with event cameras. In: Proceedings of the IEEE/CVF conference on computer vision and pattern recognition, 13884–13893.

Gu A., Dao T., 2023. Mamba: Linear-time sequence modeling with selective state spaces. [arXiv preprint](https://arxiv.org/abs/2306.08001)

arXiv:2312.00752.

Gu C., Learned-Miller E., Sheldon D., Gallego G., Bideau P., 2021. The spatio-temporal poisson point process: A simple model for the alignment of event camera data. In: Proceedings of the IEEE/CVF International Conference on Computer Vision, 13495–13504.

Huang Z., Sheng Z., Ma C., Chen S., 2024. Human as AI mentor: Enhanced human-in-the-loop reinforcement learning for safe and efficient autonomous driving. *Commun Transp Res*, **4**, 100127.

Jiang J., Zhou X., Wang B., Deng X., Xu C., Shi B., 2024. Complementing event streams and rgb frames for hand mesh reconstruction. In: Proceedings of the IEEE/CVF Conference on Computer Vision and Pattern Recognition, 24944–24954.

Jiang Z., Xia P., Huang K., Stechle W., Chen G., Bing Z., et al., 2019. Mixed frame-/event-driven fast pedestrian detection. In: 2019 International Conference on Robotics and Automation (ICRA), 8332–8338.

Khanam R., Hussain M., 2024. Yolov11: An overview of the key architectural enhancements. [arXiv preprint arXiv:2410.17725](https://arxiv.org/abs/2410.17725).

Kim J., Bae J., Park G., Zhang D., Kim Y. M., 2021. N-imagenet: Towards robust, fine-grained object recognition with event cameras. In: Proceedings of the IEEE/CVF international conference on computer vision, 2146–2156.

Lagorce X., Orchard G., Galluppi F., Shi B. E., Benosman R. B., 2016. Hots: a hierarchy of event-based time-surfaces for pattern recognition. *IEEE Trans Pattern Anal Mach Intell*, **39**, 1346–1359.

Li D., Tian Y., Li J., 2023. Sodformer: Streaming object detection with transformer using events and frames. *IEEE Transactions on Pattern Analysis and Machine Intelligence*, **45**, 14020–14037.

Li J., Dong S., Yu Z., Tian Y., Huang T., 2019. Event-based vision enhanced: A joint detection framework in autonomous driving. In: 2019 IEEE International Conference on Multimedia and Expo (ICME), 1396–1401.

Li Y., Yang Y., Lei Z., 2024. RCTrans: Radar-Camera Transformer via Radar Densifier and Sequential Decoder for 3D Object Detection. [arXiv preprint arXiv:2412.12799](https://arxiv.org/abs/2412.12799).

Liao H., Shen H., Li Z., Wang C., Li G., Bie Y., et al., 2024. Gpt-4 enhanced multimodal grounding for autonomous driving: Leveraging cross-modal attention with large language models. *Commun Transp Res*, **4**, 100128.

*Res*, **4**, 100116.

Lin T.-Y., Dollar P., Girshick R., He K., Hariharan B., Belongie S., 2017. Feature pyramid networks for object detection. In: 2017 IEEE Conference on Computer Vision and Pattern Recognition (CVPR), 2117–2125.

Lin T.-Y., Maire M., Belongie S., Hays J., Perona P., Ramanan D., et al., 2014. Microsoft COCO: Common Objects in Context. In: Computer Vision – ECCV 2014, Lecture Notes in Computer Science, 740–755. [http://dx.doi.org/10.1007/978-3-319-10602-1\\_48](http://dx.doi.org/10.1007/978-3-319-10602-1_48).

Liu B., Xu C., Yang W., Yu H., Yu L., 2023a. Motion robust high-speed light-weighted object detection with event camera. *IEEE Trans Instrum Meas*, **72**, 1–13.

Liu S., Qi L., Qin H., Shi J., Jia J., 2018. Path aggregation network for instance segmentation. In: Proceedings of the IEEE conference on computer vision and pattern recognition, 8759–8768.

Liu Z., Cheng J., Fan J., Lin S., Wang Y., Zhao X., 2023b. Multi-modal fusion based on depth adaptive mechanism for 3d object detection. *IEEE Transactions on Multimedia*, **27**, 707–717.

Liu Z., Li Y., Wang Y., Gao B., An Y., Zhao X., 2024a. Boosting visual recognition in real-world degradations via unsupervised feature enhancement module with deep channel prior. *IEEE Transactions on Intelligent Vehicles*, **9**, 7208–7221.

Liu Z., Qi M., Shen C., Fang Y., Zhao X., 2021. Cascade saccade machine learning network with hierarchical classes for traffic sign detection. *Sustain Cities Soc*, **67**, 102700.

Liu Z., Shen C., Fan X., Zeng G., Zhao X., 2020. Scale-aware limited deformable convolutional neural networks for traffic sign detection and classification. *IET Intell Transp Syst*, **14**, 1712–1722.

Liu Z., Yang N., Wang Y., Li Y., Zhao X., Wang F.-Y., 2024b. Enhancing traffic object detection in variable illumination with rgb-event fusion. *IEEE Trans Intell Transp Syst*, **25**, 20335–20350.

Ma C., Xue F., 2024. A review of vehicle detection methods based on computer vision. *J Intel Connect Veh*, **7**, 1–18.

Maqueda A. I., Loquercio A., Gallego G., García N., Scaramuzza D., 2018. Event-based vision meets deep learning on steering prediction for self-driving cars. In: Proceedings of the IEEE conference on computer vision and pattern recognition, 5419–5427.

Paredes-Vallés F., Hagenaars J., Croon G., 2021. Self-supervised learning of event-based optical flow

with spiking neural networks. *Adv Neural Inf Process Syst*, **34**, 7167–7179.

Paredes-Vallés F., Scheper K. Y., De Wagter C., De Croon G. C., 2023. Taming contrast maximization for learning sequential, low-latency, event-based optical flow. In: Proceedings of the IEEE/CVF International Conference on Computer Vision, 9695–9705.

Park P. K., Cho B. H., Park J. M., Lee K., Kim H. Y., Kang H. A., et al., 2016. Performance improvement of deep learning based gesture recognition using spatiotemporal demosaicing technique. In: 2016 IEEE International Conference on Image Processing (ICIP), 1624–1628.

Peng Y., Li H., Zhang Y., Sun X., Wu F., 2024. Scene adaptive sparse transformer for event-based object detection. In: Proceedings of the IEEE/CVF Conference on Computer Vision and Pattern Recognition, 16794–16804.

Rizzo C. P., 2024. Exploration of event-based camera data with spiking neural Networks.  
<https://orcid.org/0000-0003-3553-9551>.

Shiba S., Aoki Y., Gallego G., 2022. Secrets of event-based optical flow. In: European Conference on Computer VisionSpringer, 628–645.

Sironi A., Brambilla M., Bourdis N., Lagorce X., Benosman R., 2018. HATS: Histograms of averaged time surfaces for robust event-based object classification. In: Proceedings of the IEEE conference on computer vision and pattern recognition, 1731–1740.

Tian Y., Ye Q., Doermann D., 2025. Yolov12: Attention-centric real-time object detectors.  
<https://doi.org/10.48550/arXiv.2502.12524>.

Tomy A., Paigwar A., Mann K. S., Renzaglia A., Laugier C., 2022. Fusing event-based and rgb camera for robust object detection in adverse conditions. In: 2022 International Conference on Robotics and Automation (ICRA), 933–939.

Wan Z., Tan G., Wang Y., Zhai W., Cao Y., Zha Z.-J., 2024. Event-Based Optical Flow via Transforming Into Motion-Dependent View. *IEEE Trans Image Process*, **33**, 5327–5339.

Wang L., Zhang X., Qin W., Li X., Gao J., Yang L., et al., 2023. Camo-mot: Combined appearance-motion optimization for 3d multi-object tracking with camera-lidar fusion. *IEEE Trans Intell Transp Syst*, **24**, 11981–11996.

Wang Z., Li C., Xu H., Zhu X., 2024. Mamba YOLO: SSMSs-based YOLO for object detection. [arXiv](https://arxiv.org/abs/2401.01234)

preprint arXiv:2406.05835.

Yang N., Wang Y., Liu Z., Li M., An Y., Zhao X., 2025. SMamba: Sparse Mamba for Event-based Object Detection. In: Proceedings of the AAAI Conference on Artificial Intelligence, 9229–9237.

Ye C., Mitrokhin A., Fermüller C., Yorke J. A., Aloimonos Y., 2020. Unsupervised learning of dense optical flow, depth and egomotion with event-based sensors. In: 2020 IEEE/RSJ International Conference on Intelligent Robots and Systems (IROS), 5831–5838.

Zhou Z., Wu Z., Boutteau R., Yang F., Demonceaux C., Ginhac D., 2023. Rgb-event fusion for moving object detection in autonomous driving. In: 2023 IEEE International Conference on Robotics and Automation (ICRA), 7808–7815.

Zhu A. Z., Yuan L., Chaney K., Daniilidis K., 2018a. EV-FlowNet: Self-supervised optical flow estimation for event-based cameras. <https://doi.org/10.48550/arXiv.1802.06898>.

Zhu A. Z., Yuan L., Chaney K., Daniilidis K., 2018b. Unsupervised event-based optical flow using motion compensation. In: Proceedings of the European Conference on Computer Vision (ECCV) Workshops, 0–0.

## Author biography



**Zhanwen Liu** received the B.S. degree from Northwestern Polytechnical University, Xi'an, China, in 2006, the M.S. and the Ph.D. degrees in traffic information engineering and control from Chang'an University, Xi'an, China, in 2009 and 2014, respectively. She is currently a Professor with School of Information Engineering, Chang'an University. Her research interests include motion perception, behavior prediction, and data-closed-loop autonomous driving testing.



**Yujing Sun** received the B.S. degree from Chang'an University, Xi'an, China in 2023 and is currently pursuing the M.S. degree in computer science and technology in Chang'an University. Her current research interests include object detection and optical flow estimation based on event cameras and their applications in autonomous driving perception.



**Yang Wang** received the B.S. degree from Chang'an University, Xi'an, China, in 2016, and the Ph.D. degree in control science and engineering from the University of Science and Technology of China, in 2021. He is currently an Associate Professor with the School of Information Engineering, Chang'an University, Xi'an, China. His central research interests focus on computer vision and multimedia processing.



**Nan Yang** received the B.S. degree from Chang'an University in Xi'an, China, in 2022, where he is currently working toward the Ph.D. degree in traffic information engineering and control. His current research interests include object detection and multiple-object tracking based on event cameras, and their applications in intelligent vehicle and road infrastructure perception.



**Shengbo Eben Li** received the M.S. and Ph.D. degrees from Tsinghua University in 2006 and 2009, respectively. Before joining Tsinghua University, he has worked at Stanford University, University of Michigan, and UC Berkeley. His active research interests include intelligent vehicles and driver assistance, deep reinforcement learning, optimal control and estimation, etc.



**Xiangmo Zhao** received the Ph.D. degree from Chang'an University, Xi'an, China, in 2003. He is currently a Distinguished Professor with the School of Information Engineering, Chang'an University, and also is the President of Xi'an University of Architecture and Technology. He currently serves as the Vice Chairman of the China Society of Automotive Engineers. His current research interests include testing of connected vehicles, automated vehicles, and intelligent transportation systems.